Universitat Autònoma de Barcelona

Institut de Ciència de Materials de Barcelona (ICMAB-CSIC)

Nanopto

On Improving the Efficiency of Organic Photovoltaic Devices: Novel Strategies

Martí Gibert Roca

Under the supervision and tutoring of:

Mariano Campoy Quiles

Submitted in part fulfilment of the requirements
for the degree of Doctor of Philosophy in Materials Science
of the Universitat Autònoma de Barcelona, February 2022

Contents

List of Tables

List of Figures

Chapter 1

Materials and Methods

Abstract

This chapter describes the general procedures used in the fabrication and characterization of the various devices manufactured within this thesis. More specifically, it focuses on solar cell fabrication and characterization, including used materials, manufacturing techniques, and characterisation equipment. Special emphasis is placed on the modified solution-process techniques developed within our group, used to manufacture both extremely thick active layers and active layer gradient devices. The latter is especially advantageous for the manufacturing of a wide range of active layer thickness within one device, resulting in reduced material usage and accelerated device optimization. On the other hand, this chapter also describes the procedures used to manufacture NIL stamps and their role in solar cell and photodetector active layer nanostructuring, further discussed in Chapter ??. Finally, the characterization section is focused on the explanation of generally available techniques, while novel measurement procedures developed within the scope of this thesis have been thoroughly described within their corresponding chapters.

The objective of this chapter is not to deeply instruct the reader on each process and technique, but rather to provide the reader with brief explanations that can be useful in understanding

unfamiliar methods. However, we have added every possible detail about the materials and the equipment used in this thesis for the sake of completion.

1.1   Organic Solar Cell Fabrication

In this work we have focused on devices fabricated using the inverted architecture, where the transparent electrode is in contact with the electron transport layer (ETL), and the top metallic electrode contacts the hole transport layer. Because in this thesis a couple devices have been manufactured with a conventional architecture, and for the sake of completion, this explanation will be independent of device architecture, since the general fabrication procedure is the same the only difference being the ETL and HTL order and materials.

As we can see in Figure 1.1, solar cell fabrication begins with ITO covered glass substrate cleaning, according to the cleaning procedure. On top of the pristine ITO layer we deposit the first charge selective layer (ETL for inverted and HTL for conventional architecture) via solution processing, using different materials and deposition techniques, further explained in later sections according to the specific device. After the charge selective layer, a photoactive layer is deposited, also with solution processing techniques, using a wide variety of materials specified within each chapter. In the case of nanostructured devices, nanoimprinting lithography is performed on the active layer, either directly after deposition or after the solvent has had time to completely evaporate. On top of these layers, the second charge transport layer (HTL for inverted and ETL for conventional architecture), and the back electrode (high work function metal for inverted and low work function metal for conventional architecture) are deposited via thermal evaporation.

Most devices have an extra step involving the encapsulation of the entire device to prevent environment related degradation, as well as a thermal annealing that modifies their crystalline properties.
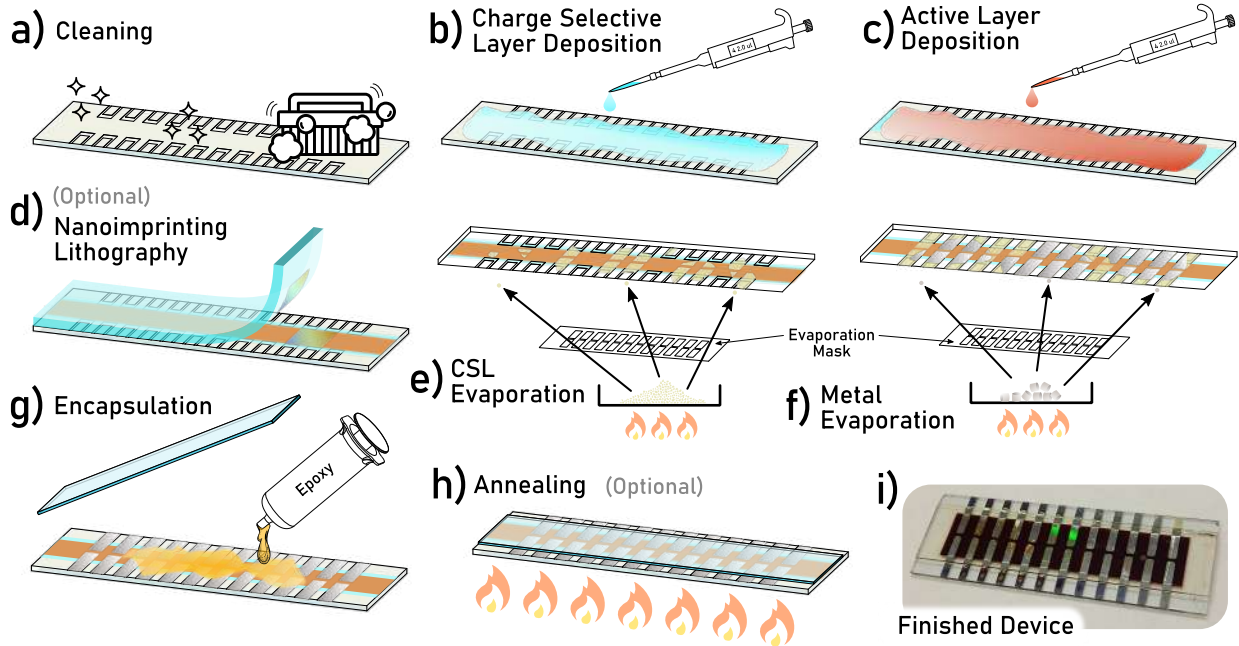
Figure 1.1: Full generic organic solar cell fabrication process with both required and optional steps clearly depicted in their chronological fabrication order.

After a device is completely finished, it is thoroughly characterized by using a variety of techniques that help us determine their electrical and optical performance, as well as their basic topographical characteristics.

1.1.1 Materials

Substrates

The substrates used throughout this thesis consist of a 1.1 mm thick glass slide, covered with a 100 nm ITO layer with a conductivity of 20 $\Omega/\square$. Various different substrate sizes and distributions have been used to adapt experiments to our specific needs (Figure 1.2).

The biggest substrate has a rectangular shape (7.5 x 2.5 cm) ever so slightly smaller than most glass slides, and it is used as a pre-scale up substrate.[1] The ITO layer of this substrate is patterned (Figure 1.2 (Patterned ITO)), allowing us to manufacture 12 individual devices on each side of the slide, each one with an active area of 8 mm^2, resulting in a total of 24
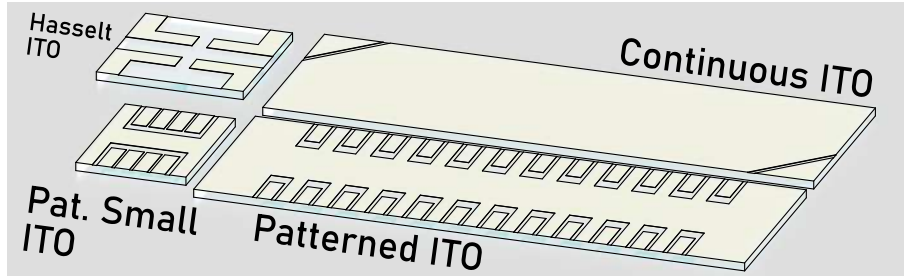
Figure 1.2: Different substrate types used throughout this thesis with their various ITO coverage patterns.

devices per substrate. We have taken advantage of this great number of devices to accelerate our research by changing various parameters (thickness, nanoimprinting depth, material...) within one single substrate, resulting in much lower material use and faster characterization times.

A slight variation on this substrate is the continuous ITO substrate, where the ITO layer covers the entire microscope slide homogeneously.[2] These substrates have been used to manufacture continuous electrode solar cells, mainly for photocurrent mapping purposes (Figure 1.2 (Continuous ITO)).

Besides these big substrates, we have also used smaller 8 pixel spin coater friendly substrates in multiple experiments.[3] The main difference between these and the previous ones is their smaller size and lower amount of pixels per substrate (Figure 1.2 (Patterned Small ITO)).

Finally, we used an additional unconventional ITO patterned device that was specifically manufactured for the group of Koen Vandewal at Hasselt University. This substrates only had 4 pixels (Figure 1.2 (Hasselt ITO)).

Electrode Materials

Front electrode transparent ITO substrate coatings were 100 nm thick with a conductivity of 20 $\Omega/\square$ for the ones provided by Ossila[1–3] and a conductivity of 10-15 $\Omega/\square$ for the ones provided by "BIOTAIN HONG KONG" to Hasselt University.

Back electrode materials include Ag (99.99% shot), Au (99.999% shot) and Ca (99% 3 mm pieces), all thermally evaporated from pellets provided by Kurt J. Lesker.

Electron and hole transport layer Materials

In inverted solar cells:

Two different ZnO formulations have been used as ETL within this work: A ZnO nanoparticle dispersion (N-10 Avantama) in isopropanol (IPA) and a ZnO sol gel solution, chemically synthesised by using recipe described by Tiwari et al.[4]

The hole transport layer was thermally evaporated Molybdenum trioxide (MoO3 99.9995% powder) from Alfa Aesar.

In conventional solar cells:

The HTL was blade coated onto the substrates using a PEDOT:PSS solution purchased from Heraeus (Clevios™ - PEDOT:PSS). The ETL was thermally evaporated onto the active layer using LiF (99.85% (metals basis)) in powder form from Alfa Aesar.

Solvents

Every solvent used for blend solution preparation was purchased from Merk (Sigma Aldrich). The solvents were used as is, without any further treatment. Used solvents were chlorobenzene (CB) , o-dichlorobenzene (DCB), toluene and o-xylene (all being ACS reagent grade). Solvents used for cleaning purposes such as acetone, 2-propanol and ethanol were purchased from Labbox and were labeled as General Laboratory Reagent (GLR).

Active Layer Materials

The active layers used during this thesis mostly consist of a blend between an electron acceptor material and an electron donor material. All active layer materials used in this work are commercially available, purchased from a variety of providers.

List of used materials:

- **Donors:**
- - P3HT (Regioregular, electronic grade 99.995% mn = 30000-60000 (Merk))
- - PBTTT (One Material Lot#YY7096)
- - PBDB-T (One Material Lot#YY16128CH)
- - PBDB-T-2Cl (One Material Lot#YY15156CH)
- - PBDB-T-2F (One Material Lot#MY7206CH100)
- - PTB7-Th (Ossila mw 57183)
- **Acceptors:**
- - PC60BM (Sigma Aldrich Lot#MKBK5229V)
- - PC70BM (Ossila >99%)
- - ITIC (One Material Lot#DW3215)
- - O-IDTBR (One Material Lot#DW4035P)
- - Y6 (One Material Lot#DW6034P)
- - ITIC-4F (One Material Lot#DW4108P)
- - O-IDFBR (One Material Lot#YY12077)
- - EH-IDTBR (One Material Lot#YY12076)
- - IO-4Cl (One Material Lot#QL21061P)
- - COTIC-4F (One Material Lot#DW7206P)

Specific solution preparation parameters, such as material concentration and ratio, varied significantly between experiments so they will be specified within each chapter. The only common step was to dissolve the materials in a solvent and stir them overnight at 80°C.

1.1.2   Cleaning

Every substrate used in this thesis was thoroughly cleaned before solar cell fabrication to ensure proper electrical contact and wettability. The substrates were cleaned by sequentially immersing
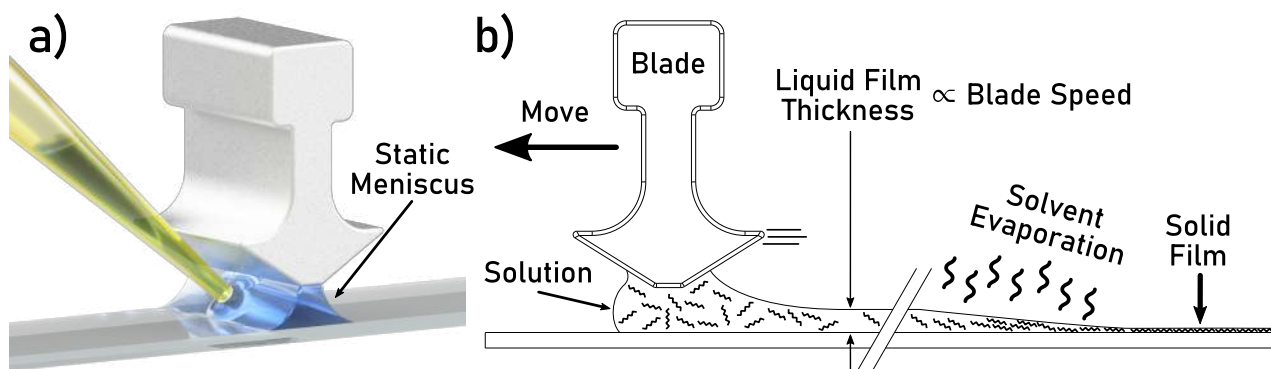
Figure 1.3: (a) Blade coating meniscus formation between blade and substrate after solution deposition. (b) Blade coating working principle, with liquid film formation, solvent evaporation and subsequent solid film formation.

them for 5 min in ultrasonication baths with different cleaning solutions, rinsing them with water in between baths to minimize bath contamination. The cleaning bath solutions were, in this order: acetone, 2% vol. Hellmanex solution in H_2O, isopropanol and 10% w/v NaOH in an aqueous solution. Finally, substrates were dried with compressed air.
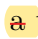
As an additional step, some substrates were treated with UV-ozone for 20 min to further improve wettability. This whole cleaning procedure was optimized during this work, with several upgrades being designed and manufactured to enhance cleaning procedure performance.

1.1.3 Blade Coating Deposition

Blade-Coating deposition, is a solution deposition method widely used within research in the field of organic electronics in general, and specially in organic photovoltaics,[5,6] mainly because of its scale-up potential and because it is usually regarded as a previous step for large scale manufacturing.[7] In this thesis it has been used as the main manufacturing method for depositing most of the solution processed layers in a variety of OPV devices.

In Figure 1.3 we can see a simplified sketch that depicts the typical process in a schematic way. A droplet with a specific volume of solution is placed within the gap between the blade and the substrate, ideally wetting both and forming meniscus on either side of the blade. Afterwards,

the blade is moved forward at a constant speed by a motor, and shear forces modify the liquid meniscus shape behind the blade. The blade motion evenly distributes the liquid along the substrate, with the thickness being directly proportional to meniscus volume, which itself is proportional to blade speed. The drying process is mainly governed by the temperature of the substrate, placed on a regulable heated platform, and air currents around the substrate, which promote evaporation.

There have been several studies relating the resulting layer thickness with the various parameters involved during the blade coating process.[8,9] However, from a practical point of view, blade gap, cast volume and blade speed usually have a the most significant effect on final film thickness, the latter being the one with the strongest influence.

Since blade speed is one of the main parameters used to control layer thickness, in our group Dr. Bernhard Dörling modified a commercial blade coater unit (ZUA 2000, Zehntner) by connecting its motor controller to an Arduino, so that the blade coating motor can vary operating speeds and accelerations within one single deposition. In this way we are able to deposit gradient layers with varying thicknesses, by changing the speed of the blade during deposition, as can be seen in Figure 1.4. All active layer films with a thickness gradient were cast by decelerating the blade from 99 mm·s⁻¹ to 1 mm·s⁻¹ during the deposition across the entire substrate length (75 mm), to provide the widest possible thickness range.

This variable speed approach enables the characterization of material thickness dependent performance in a single substrate. Such a strategy can be applied to a wide variety of solution-processed layers, but in this thesis it has been mainly applied to photoactive layer optimization. In most active layers manufactured using this approach, typical thickness gradients ranged anywhere from 300 to 50 nm. Nonetheless, the exact film gradient thickness is determined by the specific solution processing parameters and the choice of donor/acceptor materials.

The reproducibility of such accelerated blade coating deposition was confirmed by our colleague Dr. Enrique Pascual. By fabricating three batches of P3HT:O-IDTBR devices with the same processing conditions on different days, he demonstrated a consistent deposition thicknesses
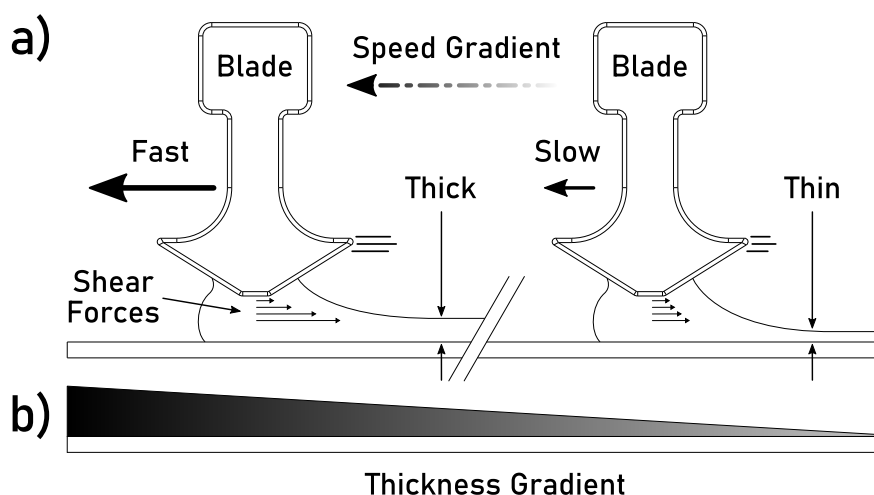
Figure 1.4: (a) Blade coating speed and liquid layer thickness relationship, related to the appearance of liquid shear forces between blade-liquid-substrate interaction. (b) Layer thickness gradient along a single substrate resulting from a controlled speed gradient during blade coating deposition.

within 5% of standard deviation, confirming the reproducibility of this novel blade deposition method.[10]

One of the caveats of regular blade coating deposition is that, for typical solution concentrations used in OPV, the thickness range is somewhat limited on the higher end, where the deposition of several μm thick films remains challenge. In this work we have developed a rather simple approach to tackle this problem where, by depositing a series of subsequent layers, we are able to fabricate very thick homogeneous films (Figure 1.5). The method relies on the speed relation between film dissolution and solvent evaporation. By blade coating a material solution on top of a dry layer made from the exact same material, if the solution is concentrated enough and the substrate is hot enough, the solvent will evaporate before the dry layer has time to fully dissolve, resulting in an effective stacking of the two films with a seamless bond with good electrical properties and no layer separation. In this way, we are able to stack several films on top of each other, achieving layers with ever increasing thickness. In this work we have manufactured devices of up to 8 times the maximum thickness of a single deposition.

The main drawback of this technique is that each subsequent film has small imperfections that can stack up, so after many depositions film homogeneity can be compromised. Another small
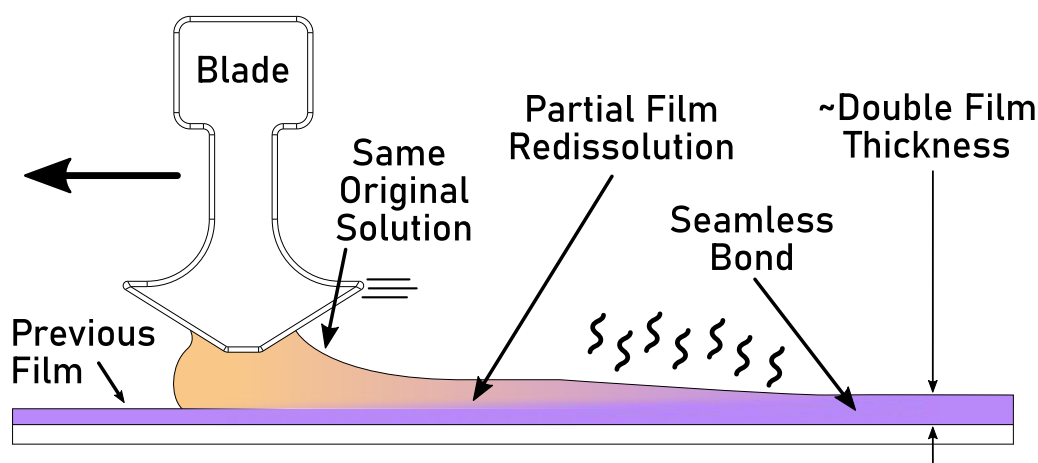
Figure 1.5: Subsequent layer deposition using the same solution for the original bottom film and the new overlaid film. The partial film redissolution aids in the formation of a seamless bond resulting in an almost twice as thick film.

inconvenience is that any gradient generated by uneven deposition can be exaggerated after subsequent film depositions. However, this can be easily mitigated by rotating the substrate by 180 degrees after each deposition. Doing this not only prevents strong gradients from forming, but evens out small gradients that might have formed during deposition.

1.1.4   Spin Coating Deposition

Spin coating deposition is a thin film coating technique that produces thin homogeneous films with a high degree of control and reproducibility, making it the most used deposition technique in the field of OPV.[5] In this thesis, this technique has been used to manufacture a limited number of devices, mainly those manufactured during my stage in Hasselt University, where blade coating was not available, encompassing the work of Chapters ?? and ??.

This technique is based on depositing a viscous fluid on a horizontal rotating surface, where the rotating motion ejects most of the solution leaving a thin and uniform liquid layer. The working solution is usually composed of a solute and a solvent, which gradually evaporates leaving the solute behind and forming an equally uniform solid film (Figure 1.6).

Common practice dictates that liquid deposition should be performed with the substrate being
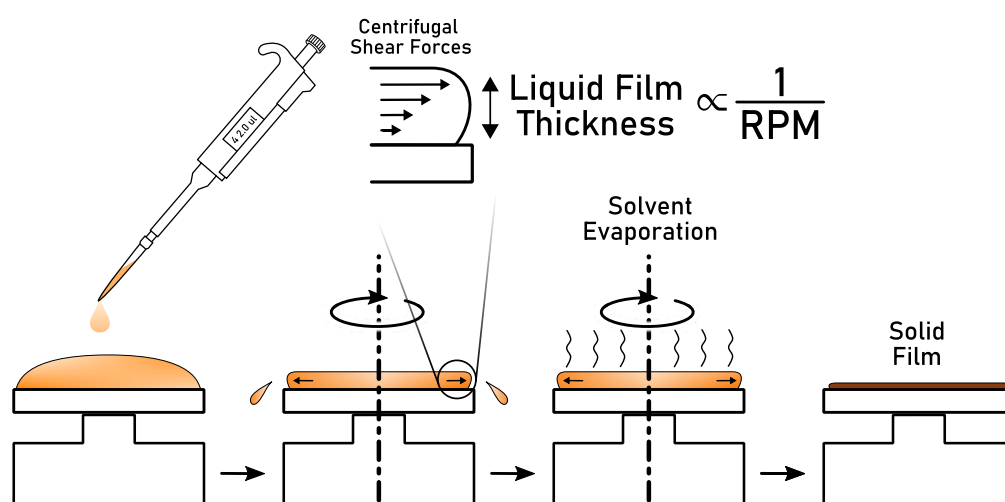
Figure 1.6: Spin Coating working principle depicting the major steps in the process with the active layer thickness and rotational speed relationship through liquid shear forces.

static or rotating at low angular velocities, a practice we call static deposition. After the liquid has covered the entire substrate, the latter is rapidly accelerated to a high angular velocity (spin speed). The adhesive forces at the liquid/substrate interface and the centrifugal forces acting on the rotating liquid result in strong sheering forces on the liquid layer, causing a radial flow in which most of the deposited solution is rapidly ejected from the substrate. Eventually these two forces equilibrate, resulting in a thin liquid film, with a highly homogeneous thickness over the entire substrate. This film is kept at a constant spinning speed to maintain film thickness during solvent evaporation, until a solid solute film is formed, with practically no solvent left. A variant of this process, commonly used for low vapour pressure solvents, consists on depositing the solution while the substrate is already spinning, a practice commonly referred to as dynamic deposition.

Over the last several decades a great deal of experimental work has been performed trying to deduce empirical correlations between experimental parameters and film thickness.[11–15] The results from these studies indicate that angular velocity, solution viscosity and solution concentration are the main driving factors determining final film thickness. On the other hand, the amount of solution initially deposited on the substrate, solution deposition rate, the history of rotational acceleration prior to final acceleration, and the total spin time have been seen to

have limited to no effect.[11]

The generalized correlation between spin coating parameters and film thickness can be described by the following, empirically derived, formula:[11]

$$h = k_2 \, \eta_0^{\beta} \, \omega^{\alpha} \tag{1.1}$$

Where h is the film thickness, η_0 is the viscosity of the deposited solution, ω is the angular velocity, α and β are empirically found exponents and k_2 is an empirically calculated constant that is strongly related to the specific polymer/solvent blend.

In a polymer solution, liquid viscosity increases at higher concentrations in a non linear manner. As a result, higher concentration solutions will lead to thicker films when spin coating at similar speeds. However, the easiest way to modify film thickness without needing to change processing parameters is to modify the angular substrate velocity, which is directly proportional to the centrifugal force. By tuning the shear force equilibrium, one can accurately control the liquid film thickness, which is directly proportional to final solid film thickness. As we can see in Figure 1.6, higher rotational speeds lead to thinner films, due to higher shear forces on the deposited liquid.

1.1.5   Thermal Evaporation

Thermal evaporation is a physical deposition technique employed in thin film deposition for multiple layers in organic photovoltaics.[16] In this thesis, this process has been used to deposit the metallic back electrode as well as the charge selective layer on top of the active layer.

The process of thermal evaporation consists on the evaporation of a coating material by heating it up in a high vacuum.[17] In the case of metals and oxides, such as the ones used in this work, this process requires the evaporation material to be at extreme temperatures in the range of 1000°C, and really high vacuum levels of around 10^{-4} Pa, due to their extremely low vapour
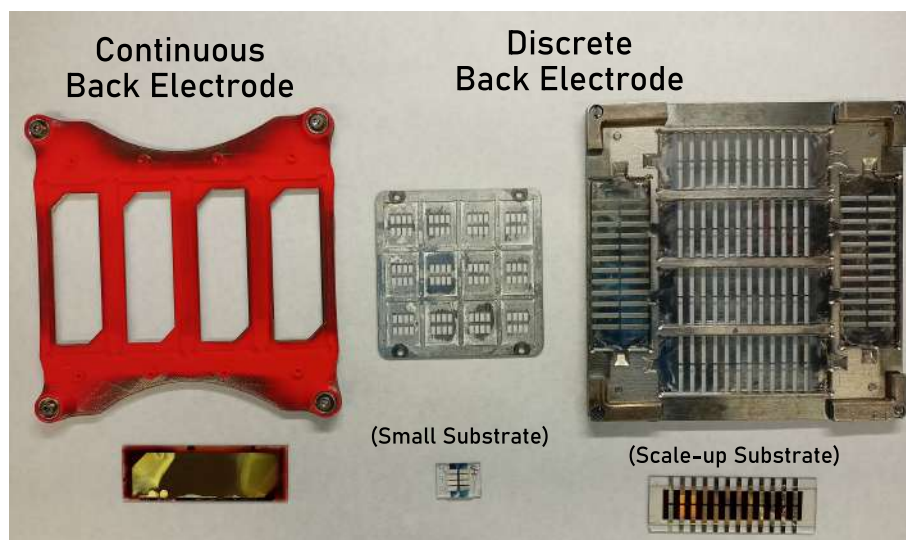
Figure 1.7: Evaporation masks used throughout this thesis for different electrode type manu-facturing, with the resulting evaporated electrodes on different devices (bottom).

pressures caused by strong atomic and molecular bonds. In order to achieve such high vacuum levels a combination of a mechanical and a turbomolecular pump are used, which are capable of maintaining stable vacuum levels of vacuum along the deposition process, pumping out any adsorbed gas released during the evaporation. Maintaining a stable vacuum is crucial for proper layer deposition, because a slight rise in pressure levels can completely stall the evaporation process.

Thermal evaporation was used to subsequently deposit the MoO3 HTL and the Ag back elec-trode through a series of custom designed shadow masks to produce different electrode distri-butions depending on the specific substrate ITO pattern (Figure 1.7). The thermal evaporator used was a ECOVap from MBraun attached to a nitrogen glovebox, and the layer thickness was measured using a quartz balance crystal.

1.1.6 Encapsulation

In order to prevent oxygen and moisture degradation, in this thesis most devices were encapsu-lated by using a UV curable epoxy resin and a glass coverslip that acted as a physical barrier for ambient oxygen and humidity. In this way, device lifetime was significantly extended, enabling

us to perform longer measurements without excessive degradation. After encapsulation, the most important remaining degradation driving factor was light.

Ideally, the used epoxy resin should not interact or affect the finished device in any way. However, general device performance is lower after encapsulation, a fact that we attribute to partial active layer blend dissolution during encapsulation, with some of the active layer components being soluble in the uncured liquid epoxy resin. Even though the active layer is mostly protected by the silver back electrode, epoxy resin can dissolve the uncovered regions surrounding the electrode, partially leeching into the solar cell active layer and hindering device performance.

In order to increase the reproducibility of the encapsulation process we designed small guides to align the substrate with the coverslip, greatly increasing device consistency, and allowing for the systematic measurement of encapsulated devices in the measurement setups discussed in following Chapters.

The epoxy was sourced from DELO, and the type is KATIOBOND LP655. The encapsulation slides were 0.5 mm glass cover slips sourced from Ossila.[18]

1.1.7   Thermal Annealing

One of the most important properties of organic electronic devices is the morphology of the organic layers. Polymers used in such layers consist of long chain molecules ~~they~~ can exhibit a wide variety of crystalline phases, as well as a varying degree of crystallinity. Organic photoactive layers usually consist of two different materials, a polymer and small molecule, which lead to a wide variety of possible crystalline states and phase segregation conditions.

Maybe the easiest approach to control these conditions in order to optimize blend morphology, is to subject organic layers to a thermal annealing process. This process consists on raising and lowering the layer's temperature in controlled steps, navigating the phase diagram in the process and modifying blend crystalline properties.

In this thesis there have been a limited number of studies focused on the effect of the annealing process on active layer morphology, further described in Chapters **?? and ??.** For thermally annealed devices, the process was carried out with a single temperature step, heating up to a certain temperature and then cooling down to room temperature, on a homogeneous temperature hotplate (SD162, Stuart), performed inside of the glovebox after device encapsulation.

1.2 Nanoimprinting Lithography

Nanoimprinting lithography is based on the more general process known as lithography, which can be generally described as a process to transfer superficial features on a mould onto any desired substrate (Figure 1.8). In this thesis, we have focused on nanoimprinting soft lithography to nanostructure the active layer of organic solar cells and organic photodetectors with the shape of a photonic crystal, in order to enhance their absorption and performance, as further described in Chapter **??**.

This process consists on transferring the superficial features of a mould onto the substrate of interest, usually resulting in a negative impression of the mould shape on the surface.[19] Feature transfer is usually achieved by placing the mould over the substrate when its material resistance to plastic deformation is low. There are multiple strategies to lower this resistance, such as heating the substrate up to the melting point, or heating it up to the glass transition and applying pressure on the mold, or even using a solvent to dissolve the substrate surface before placing the mould, and waiting for the solvent to evaporate leaving the solute with the exact mould shape.

Over the last decades, this process has been refined up to the point where nanometric features can be easily obtained with high fidelity and reproducibility. Its main advantages include mold reusability, ambient processing conditions, wide area coverage, roll-to-roll compatibility, material independence, and the fact that the smallest possible features are not diffraction limited, resulting in significantly lower operation and maintenance costs when compared with traditional
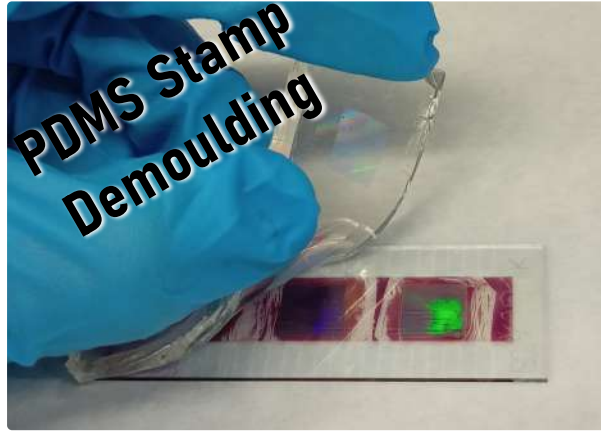
Figure 1.8: Iridescent pattern characteristic of nanostructured surfaces using lattice parameters on the same order of magnitude of visible light wavelengths. This iridescent pattern indicates the successful transfer of stamp features into the organic layer.

lithography techniques.[19] Because of all these advantages, NIL has been gaining popularity in recent years, being used in fields outside conventional semiconductor industry, such as flexible organic electronics, biocompatible materials and other experimental materials, with a variety of applications, from solar cells and metamaterials to nanofluidics and nanoelectronics.[20–23]

1.2.1   Thermal Nanoimprinting Lithography

Thermal Nanoimprinting Lithography consists on transferring mould features onto a thermoplastic substrate, by pressing it against a temperature resistant mould, while heating it above its glass transition temperature to significantly reduce its storage modulus, making plastic deformation the main deformation mechanism.[19] In this way, all the mechanical energy imparted on the substrate material will result in a permanent, non-elastic, deformation. Because of its application simplicity, in this thesis this procedure has been used to nanostructure the active layer of most devices.

The entire process consists of just four simple steps: applying pressure, heating up the substrate, cooling down the substrate, and releasing the mould (Figure 1.9). The last step being the most critical, where the mould needs to be carefully removed with a soft continuous motion to prevent damaging the newly created nanostructures. A rapid or discontinuous demoulding
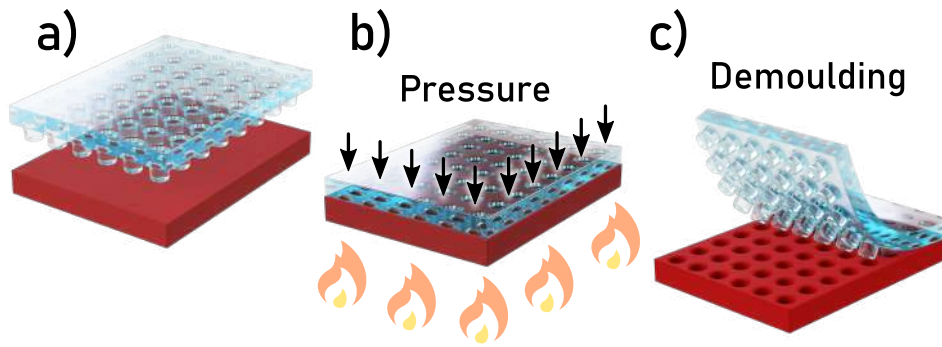
Figure 1.9: Thermally assisted nanoimprinting lithography depicting the three very basic steps involved in the process: (a) nanostructured stamp approximation, (b) combined pressure and heat for layer plastic deformation, and (c) careful demoulding.

leads to inconsistencies and defects on the nanostructures. The negative features of the mould can be immediately seen along the substrate surface after demoulding usually as an iridescent pattern (Figure 1.8).

The applied pressure will depend on material viscosity, where the weight of the mould itself is enough to transfer the features for the lowest viscosity materials, while for high viscosity materials a huge amount of force is necessary for proper feature transfer. This technique is not suitable for materials with extremely high viscosities even at high temperatures, or materials without a glass transition that degrade before their melting point, mainly because of the inability to lower their storage modulus enough for correct feature transfer.

1.2.2 Solvent Assisted Nanoimprinting Lithography

Solvent assisted nanoimprinting lithography is another variant of NIL that relies on the use of solvents to assist with feature transfer between mould and substrate. This process takes advantage of the chemical interactions between a solvent and the substrate material to temporally reduce its elasticity, promoting a plastic behaviour. Proper solvent removal is necessary before demoulding to prevent the nanostructures from disappearing after mould release. In this thesis, this process has been used in active layer nanostructuring, immediately after layer solution processing, before the solvent has had time to fully evaporate.

The process begins by exposing the substrate material to a solvent, either by directly dropping solvent onto the substrate, by exposing the substrate to solvent vapour, by wetting the mould itself, or by placing the mould onto the freshly deposited layer after solution processing. The solvent weakens the material molecular bonds and as a result the material transitions into a more malleable phase where, by pressing a nanostructured mould onto the substrate, the mould's features can be accurately transferred. The pressure needs to be maintained until the solvent is completely evaporated, in order for the substrate to regain its original stiffness. Solvent evaporation can be assisted with artificial heating and or forced air flow, after which the mould can be slowly and carefully removed to reveal the nanostructured substrate surface.

This NIL procedure is highly compatible with roll-to-roll solution processing techniques, where it can be implemented immediately after solution layer deposition, before the layer is completely dry. In this thesis, most solvent assisted NIL has been performed immediately after blade coating, on freshly deposited partially wet layers. In order to enhance the reproducibility of this technique, we developed a small accessory guide, for the moulds to be precisely located during the nanostructuring.

1.2.3   Stamp Fabrication and Architecture

The nanostructuring moulds, or stamps, used throughout this thesis are made with a curable polymer resist called Polydimethylsiloxane (PDMS), used because of its variable stiffness properties, chemical inertness, and really good feature reproduction fidelity. All stamps are exact reproductions of a "Master Stamp"; a high precision nanostructured silicon wafer that is fabricated using interference lithography. The reproduction procedure consists of several replication steps, using different materials to reduce the interaction with the delicate "Master Stamp".

The process begins with master stamp silanization, covering the silicon with a single molecule thick layer of perfluorooctyl-trichlorosilane, which acts as a release agent, preventing the silicone based replica from covalently bonding to the master. To make sure this layer is as thin as
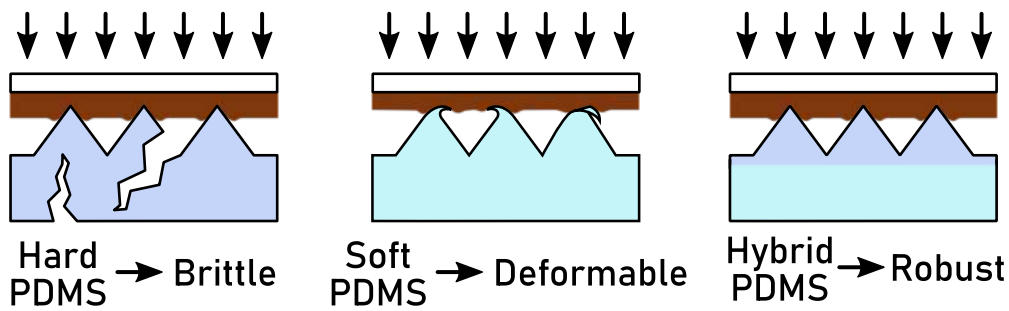
Figure 1.10: Different PDMS type stamps: Hard PDMS, which is brittle but can penetrate without problem into most active layers, even those with a high young modulus. Soft PDMS, which is really resistant to breakage but can be easily deformed by materials with high young modulus. Hybrid PDMS, which combines the best of both worlds, with a high young modulus thin layer of hard PDMS and a robust thick layer of soft PDMS that serves as a backbone.

possible, after exposing the master to a vapour of perfluorooctyl-trichlorosilane, we rinse it with acetone and heat it up to 150°C to remove the excess compound. We replicate the silanized using a thin layer of UV curable OrmoStamp® resist, which after cured over a glass substrate, following the preparation instructions, serves as a high resistance intermediate stamp for further reproduction.[24] This photocurable polymer resist has a really high young modulus (650 MPa), suitable for replicating fine structures with high aspect ratio and with excellent mechanical stability, but excessively stiff and brittle for repeated use with thermal NIL.

These OrmoStamp® masters have been replicated with PDMS, with a "Hybrid Mould" architecture, which consists on a combination of a thin layer of high stiffness (hard) PDMS, and a thick layer of low stiffness (soft) PDMS (Figure 1.10). This architecture, developed within our group, takes advantage of the high stiffness of hard PDMS, to accurately replicate the nanostructures onto hard materials, and the conformality and deformation of soft PDMS, to ensure an intimate contact between stamp and substrate during the process, and to act as a backbone for the brittle hard PDMS, limiting crack formation and stamp degradation with use. Being made from exactly the same material, the two different layers form a seamless bond, effectively becoming one single piece, even though they are manufactured in two separate steps.

Hybrid Moulds are prepared in two steps: first we mix the ingredients for hard PDMS, which are vinylmethylsiloxane and hydroxyl siloxane, the polymer precursors, Platinum(0)-1,3-divinyl-
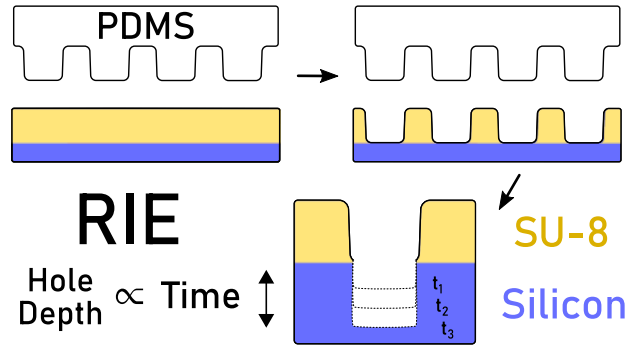
Figure 1.11: SU-8 layer on silicon substrate acting as a nanostructured mask. SU-8 covered regions are not affected by RIE, while exposed silicon regions are etched in proportion to etching time, resulting in different depth nanostructures.

1,1,3,3-tetramethyldisiloxane, the catalyst to cure the resin, 2,4,6,8-tetramethylcyclotetrasiloxane a reaction modulator, and some toluene to lower the mixture viscosity and assure proper feature reproduction. The resulting liquid is carefully poured over the silanized OrmoStamp® master, forming a thin bubble free layer that is cured at 60°C for one hour. While this is curing we prepare the soft PDMS backbone by mixing SYLGARD 184 elastomer base with its curing agent in a 10:1 ratio, thoroughly degassing the mixture. Once the hard PDMS is cured, we pour the soft PDMS mixture on top completely covering the OrmoStamp® master, and we set it to cure at 60°C for 3 hours in the oven. After the soft PDMS is completely cured, the OrmoStamp® master is carefully demoulded from the hard PDMS, leaving behind a solid stack of thin hard PDMS on the top and thick soft PDMS on the bottom, which can already be used as a nanostructuring stamp.

1.2.4   Stamp Feature Depth

The described fabrication method allows us to obtain nanostructured stamps with a variety of lattice parameters, determined by the silicon master, with a constant feature depth of around 300 nm. In this thesis, however, we required different nanostructure thicknesses, as further explained in Chapter **??**, so my colleague Dr. Molet developed and optimized a reproducible process that uses reactive ion etching to obtain stamps with variable feature depth.

This process consisted on transferring the desired features back onto a silicon substrate, by covering it with a thin layer of photocurable resin (SU-8) and nanostructuring said layer with a soft PDMS stamp with the desired features. After curing the resin, the silicon substrate was etched for different amounts of time using reactive ion etching, a highly directional etching technique, resultin in new "silicon master" moulds. These silicon masters had the same nanostructure lattice parameters as the soft PDMS, but a variety of feature depths, proportional to etching time. These were used to fabricate new shallow nanostructure PDMS stamps, used to nanostructure the polymer layer blends used in Chapter **??**.

1.3 Device Characterization

In order to assess the performance and fundamental characteristics of our devices, a variety of characterization techniques have been used throughout this thesis. The main purpose of this section is to very briefly describe the working principle of the different techniques, and to specify the equipment used in each measurement. They are arbitrarily separated between electrical characterization, where we majoritarily evaluate device performance and electrical characteristics, and optical and topological characterization, where we evaluate mostly device morphology and its light interaction characteristics.

1.3.1 Electrical Characterization

The main techniques used to electrically characterize our devices are JV-Curves, which measure current density of our device at different voltages; External Quantum Efficiency (EQE) curves, which measure the efficiency of our devices at converting incoming photons into electrons; Light Beam Induced photoCurrent (LBIC) maps, where we can evaluate the local performance of a solar cell at several positions creating an effective efficiency map; and Transient Photodiode Response, where we evaluate photodiode speed performance.

JV Characterization

In our lab, JV curves have been measured using a custom made semi-professional JV characterization setup, which includes a demultiplexing board in combination with a LabVIEW application, and has been fully developed under the umbrella of this work (further described in Chapter **??**). This setup is connected to a Keithley 2400 source meter that performs the high precision current and voltage measurements. In order to illuminate our devices, we have used a solar simulator (XES-100S, SAN-EI Electric) under AM 1.5G (Air Mass 1.5 Global) and 1000 Wm^{-2} illumination. Being AAA class, this solar simulator guarantees a homogeneous illumination area of 10 x 10 cm, which has proven to be extremely useful to characterize all our different devices, which measure up to 7.5 cm long. The solar simulator was calibrated before each experiment to ensure the measurement reliability, using a certified reference silicon solar cell (Oriel, Newport).

In this thesis JV curve measurements have been one of the main performance characterization methods, being widely used in every chapter.

External Quantum Efficiency

External quantum efficiency measurements have been performed performed on a custom made semi-automated experimental setup, with an associated LabVIEW controlling Software, fully developed under the umbrella of this work (further described in Chapter **??**). This experimental setup is coupled to a Supercontinuum laser light source and a computer-controlled monochromator (LLTF contrast, Fianium), which is further filtered to provide a continuous spectral range. With this setup we are able to illuminate the sample with light ranging from 400 nm to 1100 nm, range which can be further extended into the infrared by changing the monochromator. The current measurements were performed with a Keithley source meter 2450.

EQE measurements have been the other main performance characterization method used throughout this thesis, which have been combined with JV measurements to assess solar cell

and photodetector efficiency in every chapter.

LBIC Maps

Light Beam Induced photoCurrent (LBIC) maps are a really useful tool to assess the local performance of optoelectronic devices. To obtain such maps, the optoelectronic device is illuminated with a really concentrated beam of light, around 50 μm in our case, and, while moving the beam in a scanning pattern over the whole sample, device current is measured at each point. In this way we obtain a photocurrent map of our entire device that shows light power conversion efficiency distribution along the entire photoactive layer (Figure 1.12). This procedure is usually performed using either monochromatic or white light. However, in this work, we have modified an existing setup, connecting it to the Supercontinuum/monochromator source, so that we can illuminate the sample with any desired wavelength. As a result, we have been able to measure the performance distribution of various devices at very different wavelengths, as can be seen on Chapter ??.

LBIC measurements were performed using an experimental setup assembled within our group, mainly consisting of parts bought from Thorlabs. As stated before, the illumination source was the Supercontinuum laser light source and a computer-controlled monochromator (LLTF contrast, Fianium), while the sample was moved using Thorlabs motors (25 mm (0.98") Low-Profile Motorized Translation Stage) and the current was measured using a Keithley Source Meter 2400. The entire setup was controlled using custom made LabVIEW scripts developed within our group.

Transient Photodiode Response

In order to characterize transient photodiode response, which can be seen in Chapter ??, we slightly modified the existing EQE setup by placing a mechanical chopper in the laser light path, which temporally interrupted the photodiode illumination, allowing for an easy control
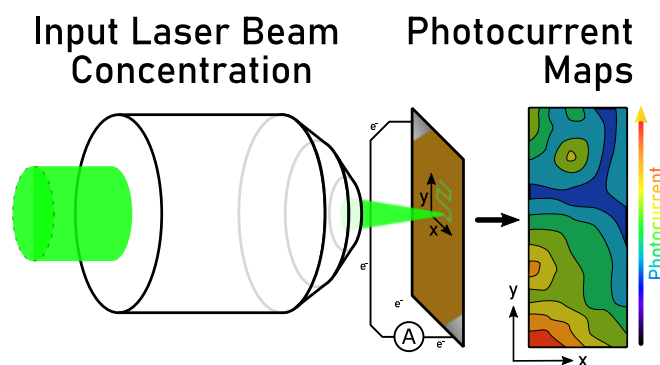
Figure 1.12: Light Beam Induced photoCurrent Map generation by scanning a laser beam focused with a microscope objective throughout a sample, while recording the photocurrent at each point.

of both illumination rate and wavelength. To characterize such fast responses we used an x brand oscilloscope, which measured the voltage drop on a 50 Ω resistor connected across the leads of the device being characterized.

1.3.2   Optical Characterization

Fourier Transform Infrared spectroscopy (FTIR)

Fourier Transform Infrared spectroscopy (FTIR) is a fast and reliable way to obtain the absorption spectra of a sample. This spectroscopic technique differs significantly from the more conventional "dispersive spectroscopy", where the sample is illuminated by one wavelength at a time, and we measure how much light is absorbed at each wavelength over a defined range. The main advantage of FTIR spectroscopy is that we shine the sample with light containing multiple wavelengths and we measure how much light is absorbed. After the first absorption measurement, the instrument changes the wavelength combination of the incoming beam and repeats the absorption measurement. This process is rapidly repeated many times over a short time span, while a computer takes the resulting interferogram and, by applying a Fourier Transform, it calculates the absorption of the sample at each wavelength. The various wavelength combinations used in this technique are the result of a combination between a broadband light

source, which covers the entire spectrum to be measured, and a Michelson interferometer.

To perform most of the absorption spectra obtained throughout this thesis, we measured both transmission and reflection spectra using a Bruker Vertex 70 FTIR spectrophotometer attached to an optical microscope (Bruker Hyperion). The microscope allowed us to accurately position the sample within the measuring spot. The spectra were recorded using a 4x objective with numerical aperture (NA) of 0.1, for both emission and collection, having a spot size of 400 μm^2. The reflectance measurements were normalized against calibration silver and gold mirrors, for visible and infrared ranges respectively, and a clean glass slide for the transmission measurements.

Integrating Sphere Spectra

An integrating sphere is an optical device used to quickly and reliably measure reflectance and transmittance spectra. This element consist of a hollow highly diffusive sphere, with lateral holes used as input and output ports, which scatters incoming light to remove spectral directionality components. There are two main measuring modes: Transmittance, where the sample is placed on the light input port, filtering incoming photons, with every other port plugged with highly diffusive plugs, which results in a transmission spectrum; and Reflectance, where the sample substitutes one of the output ports, reflecting only a certain photon fraction, resulting in a reflection spectrum. The reflection spectrum is normalized with that of a highly diffusive white material, which is considered to be 100% reflective, while the transmission spectrum can be normalized with any material, such as a glass substrate, by first measuring its transmittance and then subtracting the signal. This characterization method allowed us to measure the reflectance and transmittance spectra of several active layers of organic solar cells discussed in Chapter **??**.

In order to perform the integrating sphere measurements we used an ISP-REF Integrating Sphere coupled with a tungsten-halogen light source and a Flame spectrometer (Ocena Optics) through two optic fiber cables, all being controlled with the spectroscopy software OceanView.

1.3.3   Topological Characterization

To study the surface and thickness of our devices we decided to use two of the most commonly used techniques in material sciences, Scanning Electron Microscopy and Profilometry. These techniques give us insight on the surface topography, the layer thicknesses and the coating conformality of our devices among other information. Besides, Dr. Edgar Gutiérrez Fernández and Dr. Jaime Martín have performed both GIWAXS and GISAXS on some of our samples, characterize active layer blend morphology.

Scanning Electron Microscopy

Scanning electron microscopy (SEM) is a really powerful technique that provides close to nanometric resolution of a sample surface topology. This technique is based on accelerating electrons, collimating them into a beam, and focusing the beam onto a sample of interest. These accelerated electrons will interact with the sample in different ways, depending on the angle between the beam and the sample and its composition. By using different kinds of detectors, we can extract information about these interactions, and construct different images that provide topology and compositional information about the sample.

In Chapter ??, SEM has been extensively used to analyse nanostructure topology and to assess the conformality of the different layers on our devices. We have used a Quanta FEI 200 FEG-ESEM 53 electron microscope. For metal coated, or fairly conductive substrates, we have used the high vacuum mode (10^{-3} Pa) and voltages ranging from 10 to 15 KV. In the case of poorly conductive substrates, such as PDMS, low vacuum conditions with a 60 Pa water vapor atmosphere and voltages form 5 to 10 KV were used, to minimize the aberrations caused by surface charge build-up.
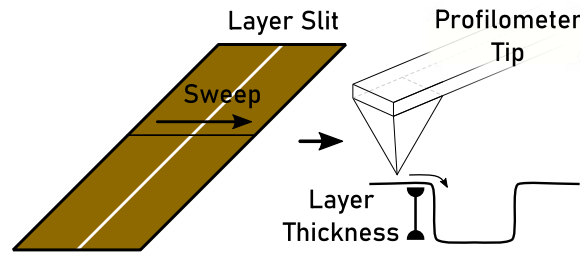
Figure 1.13: Layer with a slit inscribed on the center through which the fine tip of a profilometer is swept, in order to measure the layer thickness.

Contact Profilometry

Contact profilometry is another useful technique that provides information about surface topology with a really high resolution. The main working principle is not that different from a record player, where a needle is gently moved in close contact over a substrate surface, with a very small contact force, causing the needle to be deflected by any change in surface topology as it moves through the substrate. This needle deflection is then transduced into an electrical signal, which can be directly related to the relative height of the sample along the needle's path. This technique is able to scan features with almost nanometric vertical resolution and sub-micrometric lateral resolution.

In this work we have mainly used profilometry to determine the thickness of the various layers within our device. The easiest way to determine layer thickness is by extracting a profile cross section through a step in the layer, which we artificially create by either depositing layers with a gap on the deposited material, or by sharply scribing a gap (Figure 1.13), resulting in a slit on the layer to be measured. The equipment used was a KLA Tencor D-500 profilometer. Measurements have been performed with a diamond tip, placed in contact with the substrate applying a 0.03 mg contact force, and slowly scanning the sample at 0.1 mm s^{-1} along a specified line. This technique has been extensively used throughout Chapter **?? and ??,** to relate deposition conditions with final layer thickness, and to perform correlation studies between active layer thickness and final optoelectronic device performance.
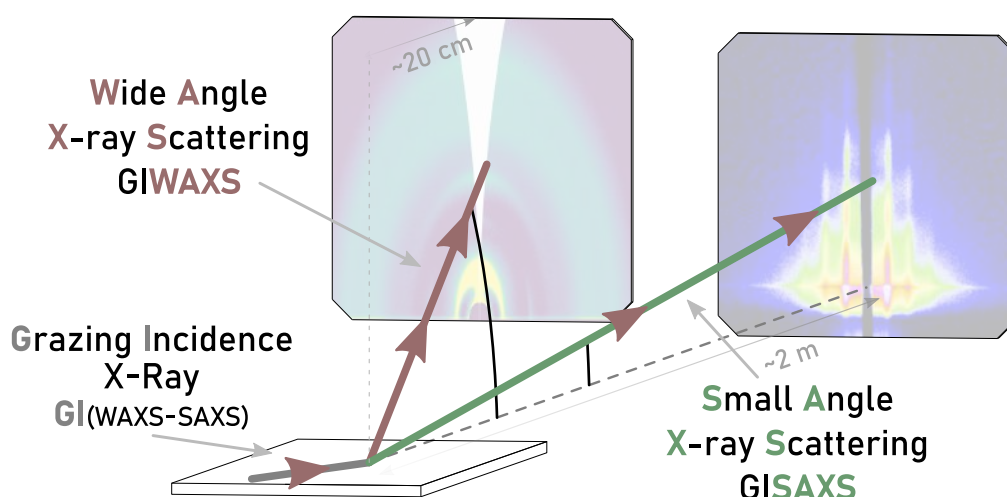
Figure 1.14: Basic detector sample distance relationship difference in GIWAXS and GISAXS.

Grazing Incidence X-Ray Scattering Characterization

Grazing incidence X-ray Scattering is a characterization technique that consists on shining an X-ray beam onto a substrate at a very low incoming angle (grazing incidence) to limit light scattering to the superficial regions, making this technique highly surface sensitive. By operating close to the film critical angle, the evanescent wave established on the film decreases fast enough to guarantee that the signal is only coming from the topmost layer, with a penetration depth on the order of nanometers. That is why this technique is widely used in thin film morphology characterization. The main limitation of this technique is that, by projecting the beam onto the surface at really low angles, even relatively collimated beams exhibit wide beam footprints, limiting local resolution. As an example a 50 μm beam at 0.1° incidence has a beam footprint of 28.6 mm, a spot 573 times bigger than the original.

This technique is further subdivided in Grazing Incidence Wide Angle X-ray Scattering (GI-WAXS) and Grazing Incidence Small Angle X-ray Scattering (GISAXS), where their main difference is the angle of diffracted light captured by the detector. There is no universally accepted border between these two regimes, but in general GIWAXS focuses on detecting the entire scattering angular range by placing the detector close to the sample, while GISAXS is

centered around detecting the weakly scattered X-rays, with the detector far away from the sample.[25] The main difference between these techniques is the length scale they are probing, where GISAXS is used on determining long range order in morphology, with smaller diffraction angles, and GIWAXS being more involved in probing atomic and molecular distances in crystal lattices.

In this thesis, both GIWAXS and GISAXS have been used to characterize temperature dependent active layer morphology of devices manufactured in Chapter **??.** The ~~entire~~ measurements, data processing and interpretation was fully performed by Dr. Edgar Gutiérrez Fernández and Dr. Jaime Martín.

GIWAXS experiments were carried out at NCD-SWEET beamline at ALBA Synchrotron (Barcelona). The samples were measured in a grazing-incidence geometry, placing the beam at an incident angle of 0.12° to probe the total volume of the film. The energy of the beam was 12.4 keV ($\lambda = 0.1$ nm) with exposure times of 1 s. The patterns were taken with the WAXS LX255-HS detector (Rayonix), placed at 20 cm from the sample position, using pixels of 88.5 x 88.5 μm^2. The 2D pixel maps were transformed into q-space and integrated using a self-made MATLAB script and pyFAI package of Python.

More info: https://www.cells.es/en/beamlines/bl11-ncd

GISAXS measurements were performed at SAXS beamline, at Elettra Sincrotrone (Trieste, Italy). Thin film samples were measured using an incoming X-ray beam at an incident angle between 0.12° and 0.15° and exposition times of 10 s. The wavelength of the X-ray beam was $\lambda = 0.154$ nm (E = 8 keV). The patterns were taken using a Pilatus 1M detectors (Dectris), with a pixel size of 172 x 172 μm^2, placed at 1200 millimeters from the sample. 2D pixel maps were transformed into q-space and integrated using a self-made MATLAB script.

Bibliography

[1] ITO Glass Substrates — PV and OLED, 20 x 15 mm — Ossila.

[2] ITO Glass Substrates — PV and OLED, 20 x 15 mm — Ossila.

[3] ITO Glass Substrates — PV and OLED, 20 x 15 mm — Ossila.

[4] D. C. Tiwari, Shailendra Kumar Dwivedi, Phukhrambam Dipak, Tarun Chandel, and Rishi Sharma. Sol-gel derived ZnO as an electron transport layer (ETL) for inverted organic solar cells. In *AIP Conference Proceedings*, volume 1832. American Institute of Physics Inc., 5 2017.

[5] Priscila Gonçalves Vasconcelos Sampaio, Mario Orestes Aguirre González, Paula de Oliveira Ferreira, Priscila da Cunha Jácome Vidal, Jonathan Paulo Pinheiro Pereira, Helder Rodrigues Ferreira, and Pedro Carlos Oprime. Overview of printing and coating techniques in the production of organic photovoltaic cells, 10 2020.

[6] Gabriel Bernardo, Tânia Lopes, David G. Lidzey, and Adélio Mendes. Progress in Upscaling Organic Photovoltaic Devices, 6 2021.

[7] Jian Cheng, Fan Liu, Zhengqiang Tang, and Yuelong Li. Scalable Blade Coating: A Technique Accelerating the Commercialization of Perovskite-Based Photovoltaics, 8 2021.

[8] M. Sajid, M. Mughees, N. Ali, and H. Shahzad. A theoretical analysis of blade coating for third-grade fluid. *Journal of Plastic Film and Sheeting*, 35(3):218–238, 7 2019.

[9] Frederik C. Krebs. Fabrication and processing of polymer solar cells: A review of printing and coating techniques, 2009.

[10] Enrique Pascual San José. *On the upscaling of organic solar cells based on non-fullerene acceptors*. PhD thesis, 2020.

[11] K. Norrman, A. Ghanbari-Siahkali, and N. B. Larsen. Studies of spin-coated polymer films, 2005.

[12] Juey H Lai. An Investigation of Spin Coating of Electron Resists. *Polymer Engineering and Science*, 19(15):1117–1121, 11 1979.

[13] Samson A Jenekhe. The Rheology and Spin Coating of Polyimide Solutions. *Polymer Engineering and Science*, 23(15):830–834, 1983.

[14] B D Washo. Rheology and Modeling of the Spin Coating Process. *IBM Journal of Research and Development*, 21(2):190–198, 1977.

[15] B. G. Higgins. Film flow on a rotating disk. *PHYS. FLUIDS*, 29(11 , Nov. 1986):3522–3529, 1986.

[16] Hongseok Youn, Hui Joon Park, and L. Jay Guo. Organic photovoltaic cells: From performance improvement to manufacturing processes. *Small*, 11(19):2228–2246, 2015.

[17] Joy George. *Preparation of Thin Films*. CRC Press, 2 1992.

[18] Glass Substrate Encapsulation Coverslips / Slides — Ossila.

[19] Stephen Chou. Nanoimprint lithography, 2 2003.

[20] Agustín Mihi, Fiona J. Beck, Tania Lasanta, Arup K. Rath, and Gerasimos Konstantatos. Imprinted electrodes for enhanced light trapping in solution processed solar cells. *Advanced Materials*, 26(3):443–448, 1 2014.

[21] Xueye Chen and Lei Zhang. Review in manufacturing methods of nanochannels of bio-nanofluidic chips, 2018.

[22] Mayte Gómez-Castaño, Juan Luis Garcia-Pomar, Luis Alberto Pérez, Sharvina Shanmugathasan, Serge Ravaine, and Agustín Mihi. Electrodeposited Negative Index Metamaterials with Visible and Near Infrared Response. *Advanced Optical Materials*, 8(19), 10 2020.

[23] Stephen Y Chou, Peter R Krauss, Wei Zhang, Lingjie Guo, and Lei Zhuang. Sub-10 nm imprint lithography and applications. Technical report, 1997.

[24] OrmoStamp. Processing Guidelines - OrmoStamp. Technical report, micro resist technology, Berlin, 11 2012.

[25] Asif Mahmood and Jin Liang Wang. A Review of Grazing Incidence Small- and Wide-Angle X-Ray Scattering Techniques for Exploring the Film Morphology of Organic Solar Cells, 10 2020.